

1 Estimating cortical thickness trajectories 2 in children across different scanners 3 using transfer learning from normative 4 models

5

6 Gaiser C. ^{a,b}, Berthet P. ^{c,d}, Kia S.M. ^{e,f,g}, , Frens M. A. ^a, Beckmann C. F. ^{e,h,i}., Muetzel R. L. ^{j,k},
7 Marquand A. ^{e,h}

8

9

10 ^a Department of Neuroscience, Erasmus MC, University Medical Centre Rotterdam, Rotterdam,
11 The Netherlands.

¹² ^b The Generation R Study Group, Erasmus MC - Sophia Children's Hospital, University Medical
¹³ Centre Rotterdam, Rotterdam, The Netherlands.

14 ^c Department of Psychology, University of Oslo, Oslo, Norway.

15 ^d Norwegian Center for Mental Disorders Research (NORMENT), University of Oslo, and Oslo
16 University Hospital, Oslo, Norway.

17 ^e Donders Institute for Brain, Cognition, and Behavior, Radboud University, Nijmegen, the
18 Netherlands

19 ^f Department of Psychiatry, Utrecht University Medical Center, Utrecht, the Netherlands.

20 ⁹ Department of Cognitive Science and Artificial Intelligence, Tilburg University, Tilburg, the
21 Netherlands.

22 ^h Department of Cognitive Neuroscience, Radboud University Medical Center, Nijmegen, the
23 Netherlands.

24 ⁱ Centre for Functional MRI of the Brain, University of Oxford, Oxford, UK.

25 ^j Department of Child and Adolescent Psychiatry, Erasmus MC - Sophia Children's Hospital,
26 University Medical Centre Rotterdam, Rotterdam, The Netherlands.

27 ^k Department of Radiology and Nuclear Medicine, Erasmus MC - Sophia Children's Hospital,
28 University Medical Centre Rotterdam, Rotterdam, The Netherlands.

29
30 * Contributed equally to this work
31
32
33

34 Keywords

35 Normative modelling

36 MRI

37 Neurodevelopment

38 Brain age

39 Cortical thickness

40 Abstract

41 This work illustrates the use of normative models in a longitudinal neuroimaging study of children
42 aged 6-17 years and demonstrates how such models can be used to make meaningful
43 comparisons in longitudinal studies, even when individuals are scanned with different scanners
44 across successive study waves. More specifically, we first estimated a large-scale reference
45 normative model using hierarchical Bayesian regression from N=40,435 individuals across the
46 lifespan and from dozens of sites. We then transfer these models to a longitudinal developmental
47 cohort (N=5,985) with three measurement waves acquired on two different scanners that were
48 unseen during estimation of the reference models. We show that the use of normative models
49 provides individual deviation scores that are independent of scanner effects and efficiently

50 accommodate inter-site variations. Moreover, we provide empirical evidence to guide the
51 optimization of sample size for the transfer of prior knowledge about the distribution of regional
52 cortical thicknesses. We show that a transfer set containing as few as 25 samples per site can
53 lead to good performance metrics on the test set. Finally, we demonstrate the clinical utility of this
54 approach by showing that deviation scores obtained from the transferred normative models are
55 able to detect and chart morphological heterogeneity in individuals born pre-term.

56

57 1. Introduction

58 Identifying structural or functional biomarkers of psychiatric and neurological illnesses across the
59 lifespan has received increasing attention in recent years. Many of these disorders present
60 symptoms that begin during childhood and adolescence (Bayer et al., 2021; Rogers & de Brito,
61 2016; Solmi et al., 2022; Whittle et al., 2020). There is however large inter-individual heterogeneity
62 in symptoms and underlying biology (DeLisi, 2008; Fuhrmann et al., 2022; Mills et al., 2021;
63 Tamnes et al., 2017), making it challenging to pinpoint the precise underlying neurobiological
64 substrates. Longitudinal datasets provide particularly valuable insights on the temporal evolution
65 of brain development and offer considerable potential to understand the emergence of
66 psychopathology and to parse this heterogeneity across individuals.

67

68 To detect and understand this heterogeneity and atypicality, there is a need to better characterize
69 typical neurodevelopment (Insel, 2014; Volpe, 2009). In recent years, the availability of large
70 datasets has greatly assisted efforts to understand inter-individual variability in brain development
71 (Bethlehem et al., 2022; Rutherford, Fraza, et al., 2022). For example, large scale studies using
72 cortical volume, cortical thickness (CT) and surface area have identified a general decrease in
73 these metrics with age, after adolescence (Bethlehem et al., 2022; Frangou et al., 2022;
74 Rutherford, Fraza, et al., 2022; Tamnes et al., 2017; Thambisetty et al., 2010). CT has been
75 shown to more accurately reflect underlying pathophysiologic mechanisms than gray matter
76 volume analysis (Clarkson et al., 2011; Hutton et al., 2009; Pereira et al., 2012; Zhao et al., 2022).
77 However, these large data resources have expanded in scale via large, long-running longitudinal
78 cohort studies. While the benefits of these large and unique cohorts are obvious, such studies
79 impose particularly difficulties. For example, data must often be aggregated across multiple study
80 centers, necessitating dealing with site effects and across developmental time scale, subjects are
81 often scanned with different scanner hardware and/or software at successive timepoints. As a

82 result, there is often little or no overlap in terms of age of participants and site effects in successive
83 acquisition waves. Such non-trivial differences across sites, scanners, and timepoints have been
84 difficult to account for statistically in analyses. Therefore, in addition to longitudinal data, novel
85 methodological tools that map inter-individual differences are needed to generate new insights.

86

87 Normative modeling approaches have recently emerged as a tool for better understanding
88 longitudinal developments with neuroimaging data (Marquand et al., 2019; Marquand, Rezek, et
89 al., 2016). These approaches produce statistical inference at the individual level, without relying
90 on strong assumptions about clustering of individuals or population structure (Antoniades et al.,
91 2021; Cole, 2012; Marquand et al., 2019). Instead, symptoms in individual patients can be related
92 to extreme deviation from the normative range (Fraza et al., 2021; Marquand, Wolfers, et al.,
93 2016; Zabihi et al., 2019). This has shown the potential to detect morphological differences in
94 patient populations which were not evident using standard techniques (Remiszewski et al., 2022).
95 Additionally, a *Hierarchical Bayesian Regression* (HBR) approach to normative modeling has
96 been shown to efficiently accommodate inter-site variation and to provide good computational
97 scaling, which is useful when using large studies, longitudinal studies, or combining smaller
98 studies together, that are acquired across multiple sites (Bayer et al., 2021; Kia et al., 2022;
99 Rutherford, Fraza, et al., 2022). It also supports federated (*i.e.* decentralized) multi-site normative
100 modeling to transfer previously trained models onto unseen sites, while benefiting from the
101 training on the large reference datasets (Kia et al., 2022; Rutherford, Kia, et al., 2022). This is
102 especially interesting given that in longitudinal studies running over several years, changes of
103 scanner hardware, software and/or scan protocols are the norm rather than the exception, which
104 generates a need to correct for the resulting scanner effects.

105

106 In this work, we provide a case study in using the transfer of prior knowledge about CT
107 distributions from normative models derived from a large reference (e.g. lifespan) cohort to better
108 estimate parameters on a smaller target (e.g. clinical) cohort. For this, we use longitudinal CT
109 data from the Generation R study (Jaddoe et al., 2006; Kooijman et al., 2016; White et al., 2018),
110 which contains data from children aged 6-17 years scanned in two different scanners, unseen by
111 the reference models. The narrow age-range makes this study a good candidate for transfer
112 learning in that it is necessary to transfer information learned from a large lifespan cohort to obtain
113 precise estimates of the slope or trajectory of developmental effects across this narrow age range.
114 This method provides important benefits: one, it allows meaningful comparison of individuals
115 scanned on different scanners, while taking advantage of previous knowledge, built from large

116 publicly available datasets to set informed hyperpriors: expected mean and variance of the
117 distribution of samples for each ROIs. This, in turn, provide three benefits to the study, one
118 providing more accurate predictions from the models thanks to the use of the mentioned informed
119 priors; second this enables to reduce the ratio of training samples necessary to learn
120 developmental trajectories for to the unseen sites, thereby enabling more participants to be
121 allocated to the test set, and thus improving statistical power (Pan & Yang, 2010). Third, we will
122 show that it provides a means to draw meaningful inferences within individuals across timepoints,
123 even when follow-up scans are derived from a different scanner. This work also aims to offer
124 some guidance on the methodology, e.g. providing empirical estimates of the number of samples
125 required for the transfer of knowledge from previous learnings and choices in transfer
126 configurations, e.g. factors included as batch effects. Finally, we provide a demonstration of the
127 clinical utility of this approach by using it to understand inter-individual differences in brain
128 morphology resulting from pre-term birth.

129
130

131 2. Methods

132 2.1 Normative modeling

133 We estimated normative models using *Hierarchical Bayesian Regression* (HBR) to predict cortical
134 thickness from age, sex and scanner site, for each *region of interest* (ROI) using the PCNtoolkit
135 python package, version 0.22 (Rutherford, Kia, et al., 2022).

136 2.1.1 Reference models

137 We assembled a large reference cohort (Kia et al., 2022) containing n=40,435 (95%) healthy
138 individuals to train the normative models before validating this model on n=2,548 controls and
139 patients (5%, stratified by sites) from a collection of mostly publicly available MRI datasets across
140 77 sites and 42,983 participants: [ABIDE-1](#), [ADHD-200](#), [CAMCAM](#), [PNC](#), [CNP](#), [HCP-Aging](#), [HCP-Dev](#), [HCP-EP](#), [OASIS](#), [OPN](#), [IXI](#), [NKI-RS](#), [UKBB](#), [ABCD](#) and [CMI-HBN](#). The reference model is
141 available on the PCNportal (<https://pcnportal.dccn.nl/>). Cortical thickness measures were
142 obtained from FreeSurfer processing (versions 5.3 or 6.0), as referred in the publications
143 associated with the datasets (Dale et al., 1999; Fischl et al., 1999, 2002; Fischl & Dale, 2000).
145 Parcellation of the brain was made with the Destrieux atlas (Destrieux et al., 2010). One normative

146 model was estimated per ROI. Linear HBR models were estimated using fixed effects of age and
147 batch (*i.e.* random) effects for site and sex. In practice, this allows each site and sex to have
148 different slopes, intercepts and variances. We included only data from the first visit when multiple
149 visits were available (*i.e.* UKBB and ABCD). Any single missing individual ROI data (less than
150 0.1% of the samples per ROI) was imputed as the site and sex specific ROI mean.

151 Estimated reference models performed well according to accuracy metrics (explained variance:
152 mean=0.44, SD=0.13, *standardized mean squared error* (SMSE): mean=0.55, SD=0.13, and
153 *mean standardized log loss* (MSLL): mean=-0.37, SD=0.14). Outputs include hyperparameters
154 defining the mean and variance of the site-specific mean effects and variance, estimated during
155 the training over the collection of datasets. This can be used as informed priors when adapting
156 the normative models to unseen target sites. These hyperparameters are adapted to the unseen
157 site using a holdout subset of the target dataset, *i.e.* the adaptation set. This allows to reduce the
158 number of samples used for adaptation while retaining a low variance of the estimations.

159

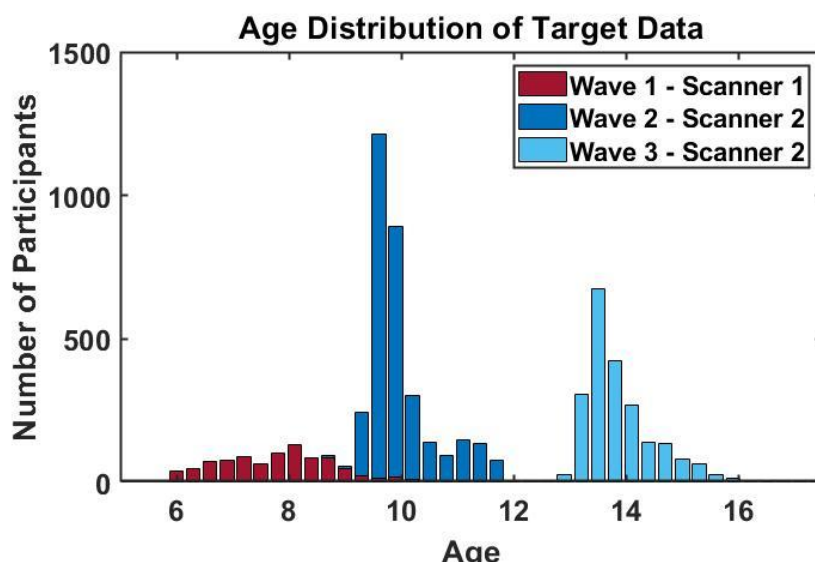
160

161 2.1.2 Target cohort

162 As target cohort, 8,523 T₁-weighted MRI scans from the population-based longitudinal Generation
163 R study (Jaddoe et al., 2006; Kooijman et al., 2016) were used. In short, the Generation R study
164 is a prospective cohort study from fetal life until adulthood that is designed to find early markers
165 for typical and atypical development, growth, and health. Almost 10,000 pregnant women living
166 in Rotterdam, the Netherlands, were enrolled in the study between 2002 and 2006. Data from the
167 children and caregivers was collected at several time points and written informed consent and/or
168 assent was obtained from all participants. The imaging protocol and quality assessment is
169 extensively described by White, Muetzel and colleagues (White et al., 2018). MRI scans were
170 acquired in 3 waves using 2 different scanners, making the cohort an ideal validation set to
171 investigate the transfer of hyperparameters from a reference dataset to an unseen target set. In
172 longitudinal studies running over several years, changes of scanner hardware, software and/or
173 scan protocols are often inevitable, which generates a need to correct for the resulting scanner
174 effects. In the first wave, 1,033 participants (484 female, age range: [6-10]) were imaged with a
175 3T MR750 Discovery MRI scanner, while in the second (n=3,920, 1,977 female, age range: [9-
176 12]) and third wave (n=3,570, 1,866 female, age range: [13-17]) a 3T MR750w Discovery scanner

177 (General Electric, Milwaukee, WI, USA) was used. After exclusion of scans with incidental findings
178 (n=58), braces (n=1067), and low-quality visual inspection ratings of FreeSurfer reconstructions
179 (n=2067), a total of 6,285 scans were included in the target dataset. Figure 1 shows a histogram
180 of age and scanner distributions in the target dataset.

181



182

183 Figure 1. Histogram of the scanning waves and age distributions in the Generation R target dataset.

184

185 2.2. Transfer of hyperparameters from reference models to target 186 cohort

187 By making use of the Generation R study cohort, we set out to show the advantage of transferring
188 the hyperparameters to an unseen site by 1) determining the optimal number of samples needed
189 for adaptation to the target cohort, 2) validating the recalibration of data to the target cohort and
190 successful removal of site-effects by comparing raw and scanner corrected values, and 3)
191 illustrating the utility of site-corrected deviations scores to uncover changes in morphology
192 between groups and individuals. In the following, these three aims are described in more detail.

193 2.2.1. Optimal sample size for parameter adaptation

194 In order to determine the optimal number of samples in the adaptation set we leveraged the large
195 amount of data available in the Generation R dataset. As described above, to prevent bias, held-

196 out data should be used for adapting the parameters of the normative model to the target cohort
197 (see Kia et al., 2020, 2022 for details). The number of scans in the adaptation set was varied
198 ranging from 5 to 300 scans and model metrics (explained variance, SMSE, MSLL) of the
199 subsequent models was calculated for each sample size. The resulting information is particularly
200 useful for small imaging cohorts, since cohorts with smaller sample sizes can employ the current
201 approach to boost power by making use of the hyperpriors inferred from large data. Yet, this is
202 only viable if the samples needed to recalibrate the models can be kept to an optimal minimum.

203 2.2.2 Validation of adaptation

204 Additionally, two aspects of the Generation R study design make the cohort an ideal target set to
205 validate the successful recalibration of the normative models to an unseen site. First, scans of
206 participants that have repeated measurements over all 3 scanning time points are present.
207 Uncorrected CT values of a participant with scans across all 3 measurement waves (and therefore
208 across both scanners) show heterogeneity over time points that is partly due to changes over time
209 and partly due to confounding site-effects. After successful recalibration of the normative model,
210 we expect resulting z-scores, which are in principle free of site-effects, of the same participant to
211 be in a similar range while raw values will differ. Second, there is an overlapping age range (8,6
212 - 10,7 years of age), in which scans from both scanners were obtained (Fig. 1). Z-scores of
213 participants from wave 1 (scanner 1), that fall in the overlapping age range of wave 1 and wave
214 2 should be distributed similarly after recalibration as z-scores in the same age range of wave 2
215 (scanner 2) while raw, uncorrected values differ due to scanner effects. Therefore, scans of
216 participants with measurements at all 3 scanning time points (n=1,317) and scans from the first
217 imaging wave that fall in the overlapping age range (n=211) were withheld from the adaptation
218 set that was used to recalibrate the reference normative model to the new unseen site. As outlined
219 above, these scans hold valuable information that will be used to determine the successful
220 calibration of the models by comparing raw CT before adaptation and corrected estimates after
221 adaptation.

222 2.2.3 Clinical application of normative estimates

223 Lastly, we used the resulting site-effect free estimates to illustrate their potential to uncover
224 morphological deviations in clinical cohorts by contrasting estimates in CT per ROI between
225 participants in the Generation R cohort born pre-term (gestational age < 37 weeks, n=339) and
226 children born at term (n=5,646). Pre-term birth interrupts a vulnerable period for brain

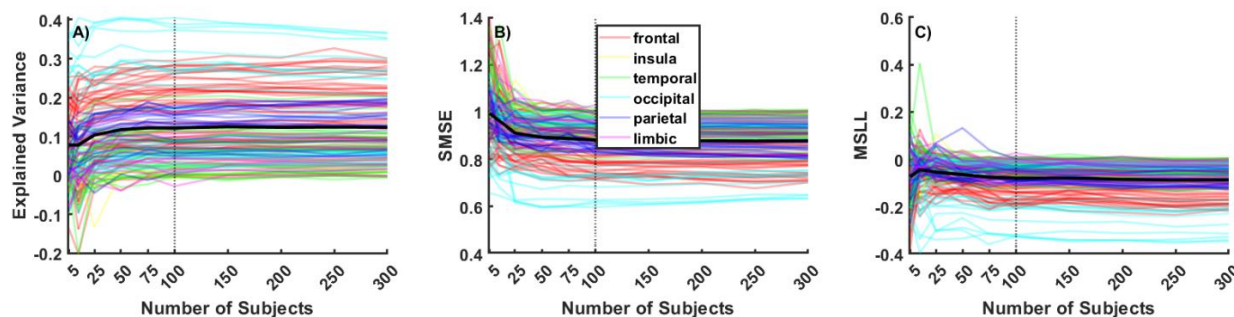
227 development, as processes such as synaptogenesis, axonal growth, and neuronal migration, take
228 place during the third semester (Volpe, 2009). Therefore, deviation scores from the normative
229 models can for instance be used to explore the variability in CT within children born pre-term, but
230 also to find ROIs that differ between children born pre-term and at term. Notably, these deviation
231 scores are free of site-effects and therefore especially suited for longitudinal MRI designs, as it is
232 the case with the Generation R study.

233 3. Results

234 3.1. Transfer results

235 3.1.1 Optimal number of samples for parameter adaptation

236 We first determined the optimal number of subjects needed in the adaptation set. Figure 2 shows
237 evaluation metrics for each ROI as the sample size of the adaptation set increases. Performance
238 of the model reaches a plateau around 100 subjects. We thus adapted the initial reference models
239 to the unseen sites of the Generation R study on n=300 (4.8%) (n=100 for scanner 1 in wave 1;
240 n=200 for scanner 2 in wave 2 and 3) and tested the models on the remaining participants
241 (n=5,985; n=813 for scanner 1 in wave 1, n=5,172 for scanner 2 in wave 2 and 3). Subjects from
242 wave 1 and 3 were sampled randomly, whereas subjects from wave 2 were sampled pseudo-
243 randomly to ensure a uniform cover of the full range of the narrow and highly peaked age
244 distribution in this wave (Fig. 1). While model performance reached a performance ceiling at
245 approximately 100 scans per scanner/wave in the adaptation sample, only slight concessions in
246 model performance are present as adaptation sample size decreases to only 25 scans.



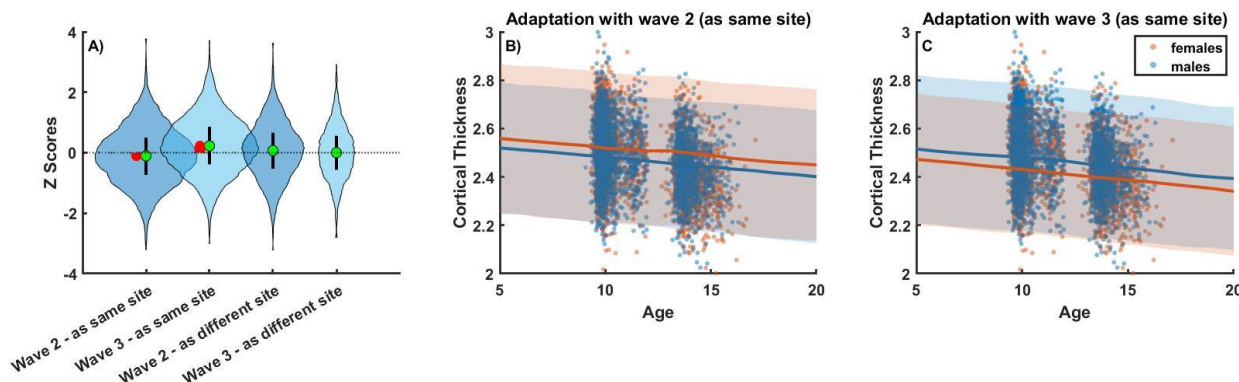
247

248 Figure 2.: Comparison of model performance as the number of subjects in adaptation set increases. Colored lines
249 show evaluation metrics per ROI, color coded according to cerebral area. The black line illustrates the mean across
250 all ROIs. Model performance reaches a plateau at approximately 100 scans per wave in the adaptation sample
251 (vertical dotted line).

252
253

254 3.1.2 Adaptation settings

255 We furthermore tested different adaptation settings. Despite the fact that scans in wave 2 and 3
256 of the target cohort were acquired on the same scanner, we compared adaptation settings treating
257 waves 2 and 3 as the same but also as different sites. When treated as same sites, we found a
258 slight bias for higher deviation scores (z-scores) when running the adaptation to a wave 2+3 test
259 set with wave 3 subjects compared to wave 2 subjects only, in particular for frontal ROIs. The
260 effect of the different adaptation settings on all ROIs is shown in Supplementary Figure 1 and is
261 explicitly illustrated in an example ROI in Figure 3. Panel A shows that the model is more
262 successful in reparametrizing the raw data to centiles when each time point of measurement is
263 handled as a separate site-effect. Possible sources for such effects might stem from changes in
264 scanner software, changes in image quality with age (i.e. motion artifacts), or sample variability.
265 In our target cohort, scanner software was upgraded after the first 370 scans of wave 2 but was
266 otherwise identical in wave 2 and wave 3. However, age-related improvements in images quality
267 are frequently reported in the literature and quality assurance, measured as topological defects
268 in the surface reconstruction for FreeSurfer processed MRI data (<https://github.com/DeepMI/qatools-python>), does show improvements in image quality with age across the three waves
269 (Mean_{wave 1}=229.06, SD_{wave 1}=98.56; Mean_{wave 2}=213.89, SD_{wave 2}=67.15; Mean_{wave 3}=166.97,
270 SD_{wave 3}=67.15).
271



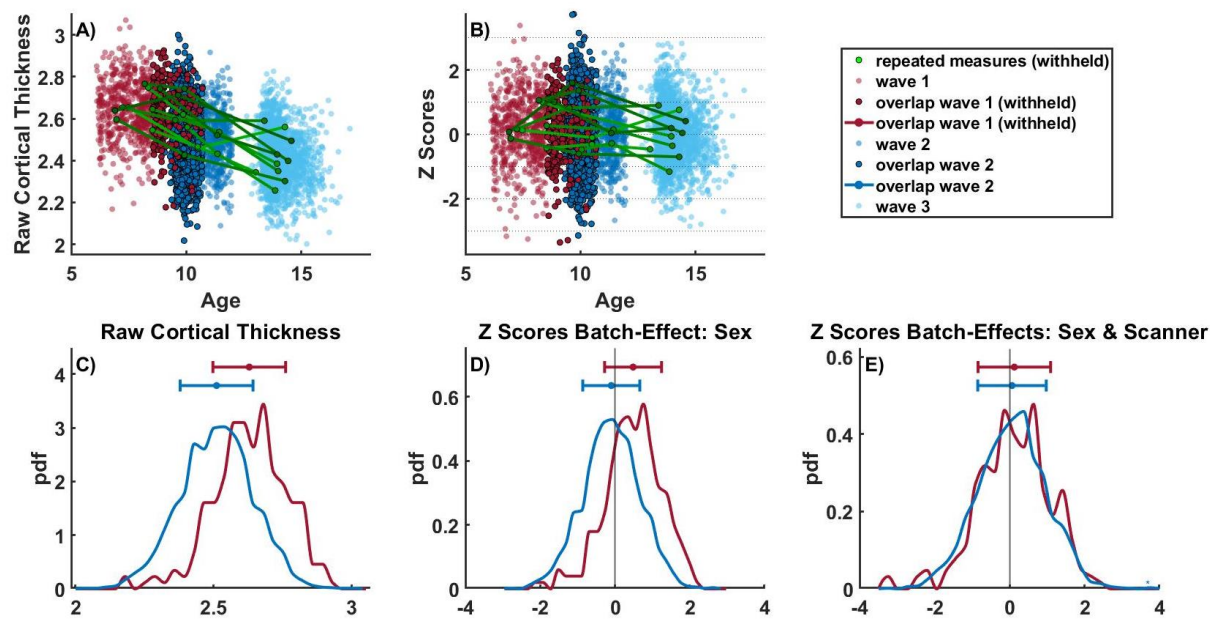
272

273 Figure 3. Effects of different recalibration configurations on the target cohort illustrated in an example ROI (inferior
274 frontal sulcus). Panel A) shows z-score distributions when measurement waves 2 and 3 of the Generation R target
275 cohort are treated as the same (same scanner) or different sites in a frontal example ROI, the inferior frontal sulcus.
276 Median and interquartile range are represented by green dots and black bars, respectively. For each measurement
277 wave, we would expect the median z-score to be around 0. However, this is not the case if measurement wave 2 and
278 3 are treated as the same site. The difference from 0 is indicated by red bars. By examining the CT trajectories in panel
279 B) and C), we see that this might be due to a misestimation of mean and variance in females when both waves are
280 treated as the same site.

281 3.1.3. Adaptation Validation

282
283 After choosing for a adaptation setting treating the three measurement waves as different batch
284 effects, we validated the success of the adaptation of the reference model to the target cohort by
285 examining the differences between raw CT values and corrected deviations (z-scores) after
286 transfer of the subjects which were withheld from the adaptation sets (Fig. 4). Scans of
287 participants with repeated measurements at all imaging waves (a random sample of ten
288 participants is depicted by green lines) show a decline over time in raw CT. As expected, thinning
289 of the cortex can be observed with age, however, the raw CT values are confounded by noise
290 stemming from site-effects of the different measurement waves. In the resulting z-scores of the
291 withheld subjects, these site-effects are removed as demonstrated by stable deviations from the
292 normative model within a participant (Fig. 4B). The same holds true for the withheld subjects from
293 measurement wave 1 that fall in the overlapping age range (8,6 - 10,7 years of age) of wave 1
294 (scanner 1) and 2 (scanner 2). While raw CT values in the overlapping age range vary vastly
295 between the two measurement waves ($t(2874)=13.4$, $p<0.001$), with a tendency of higher values
296 in measurement wave 1 compared to wave 2 (Fig. 4C), this difference is slightly reduced when
297 correcting for sex (Fig. 4D) ($t(2874)=11.4$, $p<0.001$) and practically absent in the sex- and
298 additionally site-effect corrected z-scores (Fig. 4E) ($t(2874)=1.0$, $p=0.324$). Therefore, we can
299 meaningfully compare individuals on the basis of z-scores, bearing in mind that the z-scores are
300 defined with respect to a lifespan based normative model.

301



302

303 Figure 4: Validation of transferring the reference normative model to the target cohort using two groups of subjects that
304 were withheld from the adaptation set: 1) subjects with repeated measurements at all 3 imaging waves (random sample
305 of ten participants depicted by green lines, panels A and B; 2) subjects from imaging waves 1 and 2 that fall in the
306 overlapping age range of both scanners [8,6 - 10,7] (depicted by darker shaded red and blue dots and lines, panels A-
307 E). Panel A and C show raw cortical thickness values. Panels B, D, and E show sex-effect (panel D) or sex- and site-
308 effect corrected z-scores of the same participants (panels B&E). For consistency, the same ROI (inferior frontal sulcus)
309 as in the previous figures is illustrated.

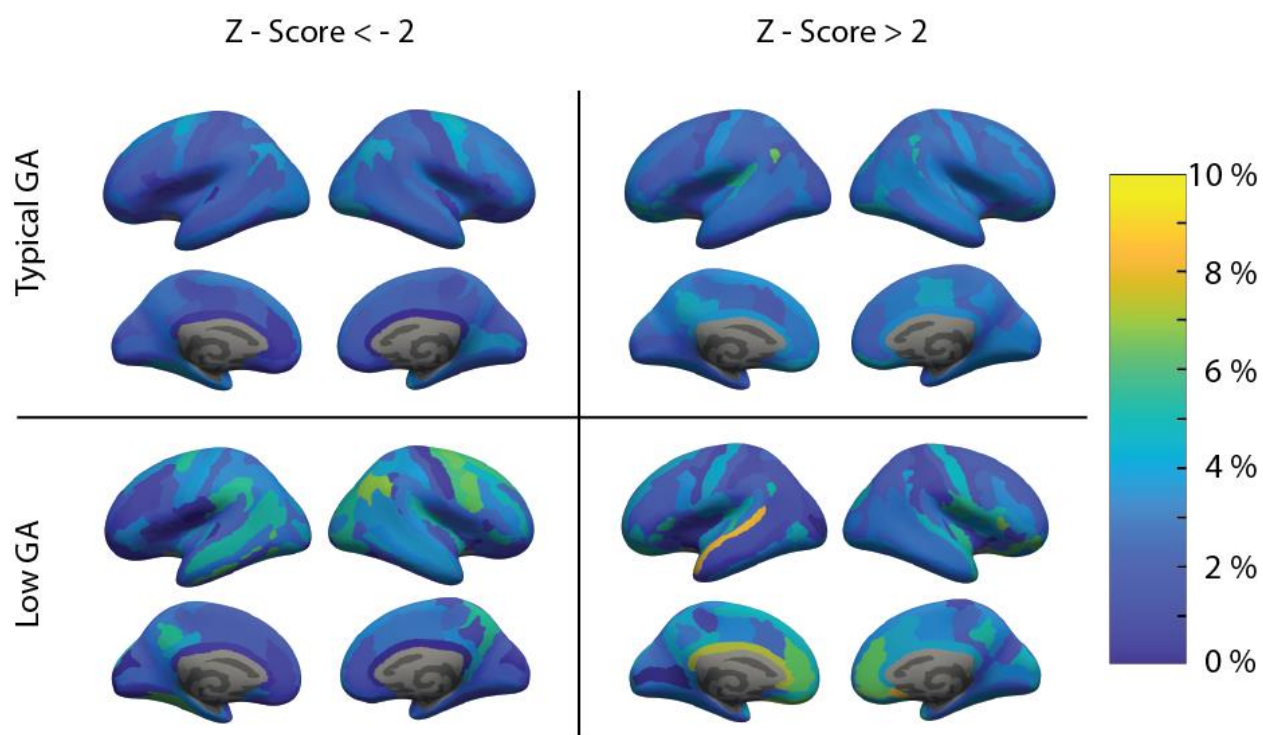
310 3.2. Relating site-effect corrected z-scores to gestational age

311 To illustrate the usefulness of the resulting models, we compared extreme deviations, acquired
312 at the level of individuals, between children born pre-term and children born at term in the target
313 cohort. Percentages of individuals with an extreme z-score (larger/smaller than 2) per ROI are
314 shown in Figure 5. In the children born at term, we find approximately 2.5% of children with
315 extreme negative and extreme positive z-scores respectively across ROIs. Exceptions are
316 primarily smaller ROIs (sulcus intermedius primus (left & right), posterior ramus of the lateral
317 sulcus (left), anterior transverse collateral sulcus (right), orbital sulcus (right)) where areas with
318 thicker cortices than expected can be observed. Importantly, extreme deviations are much more
319 prevalent with children born pre-term with the most pronounced extreme positive deviations
320 (thicker cortex than expected) found in the left pericallosal sulcus and lateral aspect of the superior
321 temporal gyrus, as well as in the anterior part of cingulate gyrus and sulcus (ACC) of both
322 hemispheres. The most striking extreme negative deviations (thinner cortex than expected) can

323 be seen on the left hemisphere in the superior and inferior temporal sulcus, lingual sulcus,
324 superior part of the precentral sulcus, supramarginal gyrus, and on the right hemisphere in the
325 superior and inferior part of the precentral sulcus, superior frontal sulcus, angular gyrus,
326 precentral gyrus and the precuneus.

327 These regions are consistent with previous findings on CT differences in adolescents born pre-
328 term. Pronounced cortical thinning has been found persistently in areas surrounding the central
329 sulcus and temporal lobes (Martinussen et al., 2005; Nagy et al., 2011; Zubiaurre-Elorza et al.,
330 2012) as well as thicker cortices in frontal regions surrounding the anterior cingulate cortex
331 (Bjuland et al., 2013). The current approach has been shown to capture structural deviations
332 better than case-control studies as they are more sensitive to individual heterogeneity
333 (Remiszewski et al., 2022). It also offers improved insights in longitudinal cohorts, as these
334 deviation scores are not confounded by site-effects.

335



336
337 Figure 5.: Differences in site-effect corrected z-scores between children born pre-term (low gestational age (GA)) and
338 children born term (typical gestational age (GA)). On the left side, extreme negative deviations (cortex thinner than
339 expected) are illustrated. On the right, extreme positive deviations (cortex thicker than expected) are shown.

340

341 4. Discussion

342 In this study, we used information from normative models that were initially trained on a large
343 number of samples, scanned over 77 sites, as prior knowledge for the parameters of the CT
344 distributions when adapting these models to the two scanners of the longitudinal Generation R
345 study.

346 We report three main findings: first, transfer learning is successful and allows for meaningful
347 comparisons between individuals from different scanners, and sexes, as previously reported (Kia
348 et al., 2022). Second, we quantified the number of samples in the transfer set needed to obtain
349 good performance metrics on the test set and show that relatively few samples are sufficient for
350 good performance (approximately n=25). This provides the added benefit of improving the
351 statistical power of statistical analyses on the resulting larger test set. While we used 100 samples
352 per measurement wave in the adaptation site, slightly smaller adaptation samples decreased the
353 evaluation metrics only marginally. Third, we show that the deviations from these normative
354 models are meaningful in that they are altered in a highly individualized manner in individuals
355 born pre-term.

356

357 Our results support the finding that normative models capture the general trend of decreasing
358 cortical thickness with age, as reported in previous studies (Bethlehem et al., 2022; Frangou et
359 al., 2022; Rutherford, Fraza, et al., 2022; Tamnes et al., 2017; Thambisetty et al., 2010).
360 Interestingly, we found that the model performed better when each measurement wave of the
361 transfer cohort was treated as a separate site-effect, even though two of three waves were
362 acquired on the same scanner. This could be due to sample variability or a misestimation of
363 parameters in the female cohort, possibly linked to the fact that scan quality tends to improve with
364 age. For future studies, it may be useful to treat distinct measurement intervals as separate batch-
365 effects, resulting in a factorial design of sex x scanners x waves, even if the scanner setup has
366 not changed, to produce more precise models. Our recommendations might differ for longer
367 timescales, non-linear or non-Gaussian lifespan trajectories, which usually requires more data
368 (de Boer et al., 2022). However, the methods we introduce can be used to determine the optimal
369 number of subjects for such cases.

370

371 The successful validation of the use of transfer learning with normative models opens the door
372 for further investigations exploring the relationship between deviation scores and various
373 phenotypes. Individual-level deviations, as obtained through normative models, have been shown

374 to provide stronger effects than typical case-control studies using uncorrected raw measurements
375 (Rutherford, Fraza, et al., 2022) and are therefore particularly suitable for exploring and
376 investigating individual differences within and across datasets. The used federated learning
377 framework makes it possible to use the models presented in this work as informed priors (models
378 are available online via PCNportal [<https://pcnportal.dccn.nl/>] to investigate CT in smaller and/or
379 clinical cohorts.

380

381 In this study, we provide an example how normative models can be used to investigate clinical
382 phenotypes, by investigating the relation between extreme deviations scores and the gestational
383 age at birth, that is between children born at-term and pre-term. While children born at-term show
384 an expected distribution of approximately 2.5% with z-scores higher than 2 or lower than -2
385 respectively, children born pre-term are more likely to have extreme deviations in specific ROIs,
386 which are consistent with previous literature showing pronounced differences in particular in
387 frontal and temporal cortices. While we show a comparison between groups, the current approach
388 does not require clustering of individuals into groups but instead can be used to make inferences
389 about heterogeneity within clinical groups as well as about deviations on an individual level.

390

391 4.1. Limitations and future directions

392 Although we demonstrate that evaluation metrics level off after 100 scans in the adaptation set,
393 as few as 25 scans can still lead to effective transfer of knowledge. However, this limitation
394 prevents small cohorts from utilizing the current approach due to the fact that the median sample
395 size of neuroimaging studies typically includes 25 participants (Marek et al., 2022).
396 Furthermore, our work estimates normative models on a single ROI, thereby neglecting any
397 spatial interdependencies between brain regions. Moreover, other image-derived phenotypes,
398 such as the cerebellum, could also be considered.

399 5. Conclusion

400 Using longitudinal cortical thickness data from the Generation R study on children aged 6 to 17
401 years old, we present an application of transfer learning of large-scale normative models which
402 produce good performance metrics with even a limited size of adaptation set. The resulting
403 deviation scores per age and ROIs, allow for meaningful comparison inter sites and inter sex.

404 Using these obtained deviation scores, we were able to show specifically localized differences in
405 cortical thickness between children born pre-term and children born at-term.
406
407

408 References

409 Antoniades, M., Haas, S. S., Modabbernia, A., Bykowsky, O., Frangou, S., Borgwardt, S., &
410 Schmidt, A. (2021). Personalized Estimates of Brain Structural Variability in Individuals with
411 Early Psychosis. *Schizophrenia Bulletin*, 47(4), 1029–1038.
412 <https://doi.org/10.1093/schbul/sbab005>

413 Bayer, J. M. M., Dinga, R., Kia, S. M., Kottaram, A. R., Wolfers, T., Lv, J., Zalesky, A., Schmaal,
414 L., & Marquand, A. (2021). Accommodating site variation in neuroimaging data using
415 normative and hierarchical Bayesian models. *BioRxiv*, 2021.02.09.430363.
416 [https://www.biorxiv.org/content/10.1101/2021.02.09.430363v2.abstract](https://www.biorxiv.org/content/10.1101/2021.02.09.430363v2%0Ahttps://www.biorxiv.org/)

417

418 Bethlehem, R. A. I., Seidlitz, J., White, S. R., Vogel, J. W., Anderson, K. M., Adamson, C.,
419 Adler, S., Alexopoulos, G. S., Anagnostou, E., Areces-Gonzalez, A., Astle, D. E., Auyeung,
420 B., Ayub, M., Bae, J., Ball, G., Baron-Cohen, S., Beare, R., Bedford, S. A., Benegal, V., ...
421 Alexander-Bloch, A. F. (2022). Brain charts for the human lifespan. *Nature*, 604(7906),
422 525–533. <https://doi.org/10.1038/s41586-022-04554-y>

423 Bjuland, K. J., Løhaugen, G. C. C., Martinussen, M., & Skranes, J. (2013). Cortical thickness
424 and cognition in very-low-birth-weight late teenagers. *Early Human Development*, 89(6),
425 371–380. <https://doi.org/10.1016/j.earlhumdev.2012.12.003>

426 Clarkson, M. J., Cardoso, M. J., Ridgway, G. R., Modat, M., Leung, K. K., Rohrer, J. D., Fox, N.
427 C., & Ourselin, S. (2011). A comparison of voxel and surface based cortical thickness
428 estimation methods. *NeuroImage*, 57(3), 856–865.
429 <https://doi.org/10.1016/j.neuroimage.2011.05.053>

430 Cole, T. J. (2012). The development of growth references and growth charts. *Annals of Human
431 Biology*, 39(5), 382–394. <https://doi.org/10.3109/03014460.2012.694475>

432 Dale, A. M., Fischl, B., & Sereno, M. I. (1999). Cortical Surface-Based Analysis. II. Inflation,
433 Flattening, and a Surface-Based Coordinate System. *NeuroImage*, 9(2), 179–194.
434 <http://linkinghub.elsevier.com/retrieve/pii/S1053811998903950%0Ahttp://surfer.nmr.mgh.h>
435 arvard.edu/ftp/articles/fischl99b-recon2.pdf

436 de Boer, A. A. A., Kia, S. M., Rutherford, S., Zabihi, M., Fraza, C., Barkema, P., Westlye, L. T.,
437 Andreassen, O. A., Hinne, M., Beckmann, C. F., & Marquand, A. (2022). Non-Gaussian
438 Normative Modelling With Hierarchical Bayesian Regression. *BioRxiv*, 2022.10.05.510988.
439 <https://doi.org/10.1101/2022.10.05.510988>

440 DeLisi, L. E. (2008). The concept of progressive brain change in schizophrenia: Implications for
441 understanding schizophrenia. *Schizophrenia Bulletin*, 34(2), 312–321.
442 <https://doi.org/10.1093/schbul/sbm164>

443 Destrieux, C., Fischl, B., Dale, A., & Halgren, E. (2010). Automatic parcellation of human cortical
444 gyri and sulci using standard anatomical nomenclature. *NeuroImage*, 53(1), 1–15.
445 <https://doi.org/10.1016/j.neuroimage.2010.06.010>

446 Fischl, B., & Dale, A. M. (2000). Measuring the thickness of the human cerebral cortex from
447 magnetic resonance images. *Proceedings of the National Academy of Sciences*, 97(20),
448 11050–11055. <https://doi.org/10.1073/pnas.200033797>

449 Fischl, B., Salat, D. H., Busa, E., Albert, M., Dieterich, M., Haselgrove, C., van der Kouwe, A.,
450 Killiany, R., Kennedy, D., Klaveness, S., Montillo, A., Makris, N., Rosen, B., & Dale, A. M.
451 (2002). Whole Brain Segmentation. *Neuron*, 33(3), 341–355. [https://doi.org/10.1016/s0896-6273\(02\)00569-x](https://doi.org/10.1016/s0896-6273(02)00569-x)

452 Fischl, B., Sereno, M. I., & Dale, A. M. (1999). Cortical surface-based analysis. I. Segmentation
453 and Surface Reconstruction. *NeuroImage*, 9(2), 195–207.
454 <http://www.ncbi.nlm.nih.gov/pubmed/9931269>

455 Frangou, S., Modabbernia, A., Williams, S. C. R., Papachristou, E., Doucet, G. E., Agartz, I.,
456 Aghajani, M., Akudjedu, T. N., Albajes-Eizagirre, A., Alnæs, D., Alpert, K. I., Andersson, M.,
457 Andreasen, N. C., Andreassen, O. A., Asherson, P., Banaschewski, T., Bargallo, N.,
458 Baumeister, S., Baur-Streubel, R., ... Dima, D. (2022). Cortical thickness across the
459 lifespan: Data from 17,075 healthy individuals aged 3–90 years. *Human Brain Mapping*,
460 43(1), 431–451. <https://doi.org/10.1002/hbm.25364>

461 Fraza, C. J., Dinga, R., Beckmann, C. F., & Marquand, A. F. (2021). Warped Bayesian linear
462 regression for normative modelling of big data. *NeuroImage*, 245(May), 118715.
463 <https://doi.org/10.1016/j.neuroimage.2021.118715>

464 Fuhrmann, D., Madsen, K. S., Johansen, L. B., Baaré, W. F. C., & Kievit, R. A. (2022). The
465 midpoint of cortical thinning between late childhood and early adulthood differs across
466 individuals and regions : Evidence from longitudinal modelling in a 12-wave sample.
467 *BioRxiv*, 261(March), 1–23. <https://doi.org/10.1016/j.neuroimage.2022.119507>

469 Hutton, C., Draganski, B., Ashburner, J., & Weiskopf, N. (2009). A comparison between voxel-
470 based cortical thickness and voxel-based morphometry in normal aging. *NeuroImage*,
471 48(2), 371–380. <https://doi.org/10.1016/j.neuroimage.2009.06.043>

472 Insel, T. R. (2014). Mental Disorders in Childhood. *JAMA*, 311(17), 1727.
473 <https://doi.org/10.1001/jama.2014.1193>

474 Jaddoe, V. W. V., Mackenbach, J. P., Moll, H. A., Steegers, E. A. P., Tiemeier, H., Verhulst, F.
475 C., Witteman, J. C. M., & Hofman, A. (2006). The Generation R Study: Design and cohort
476 profile. *European Journal of Epidemiology*, 21(6), 475–484. <https://doi.org/10.1007/s10654-006-9022-0>

477 Kia, S. M., Huijtsdens, H., Dinga, R., Wolfers, T., Mennes, M., Andreassen, O. A., Westlye, L. T.,
478 Beckmann, C. F., & Marquand, A. F. (2020). *Hierarchical Bayesian Regression for Multi-
479 Site Normative Modeling of Neuroimaging Data*. 1–12. <http://arxiv.org/abs/2005.12055>

480 Kia, S. M., Huijtsdens, H., Rutherford, S., de Boer, A., Dinga, R., Wolfers, T., Berthet, P.,
481 Mennes, M., Andreassen, O. A., Westlye, L. T., Beckmann, C. F., & Marquand, A. F.
482 (2022). Closing the life-cycle of normative modeling using federated hierarchical Bayesian
483 regression. *PLOS ONE*, 17(12), e0278776. <https://doi.org/10.1371/journal.pone.0278776>

484 Kooijman, M. N., Kruithof, C. J., van Duijn, C. M., Duijts, L., Franco, O. H., van IJzendoorn, M.
485 H., de Jongste, J. C., Klaver, C. C. W., van der Lugt, A., Mackenbach, J. P., Moll, H. A.,
486 Peeters, R. P., Raat, H., Rings, E. H. H. M., Rivadeneira, F., van der Schroeff, M. P.,
487 Steegers, E. A. P., Tiemeier, H., Uitterlinden, A. G., ... Jaddoe, V. W. V. (2016). The
488 Generation R Study: design and cohort update 2017. *European Journal of Epidemiology*,
489 31(12), 1243–1264. <https://doi.org/10.1007/s10654-016-0224-9>

490 Marek, S., Tervo-Clemmens, B., Calabro, F. J., Montez, D. F., Kay, B. P., Hatoum, A. S.,
491 Donohue, M. R., Foran, W., Miller, R. L., Hendrickson, T. J., Malone, S. M., Kandala, S.,
492 Feczko, E., Miranda-Dominguez, O., Graham, A. M., Earl, E. A., Perrone, A. J., Cordova,
493 M., Doyle, O., ... Dosenbach, N. U. F. (2022). Reproducible brain-wide association studies
494 require thousands of individuals. *Nature*, August 2022. <https://doi.org/10.1038/s41586-022-04492-9>

495 Marquand, A. F., Kia, S. M., Zabihi, M., Wolfers, T., Buitelaar, J. K., & Beckmann, C. F. (2019).
496 Conceptualizing mental disorders as deviations from normative functioning. *Molecular
497 Psychiatry*, 24(10), 1415–1424. <https://doi.org/10.1038/s41380-019-0441-1>

498 Marquand, A. F., Rezek, I., Buitelaar, J., & Beckmann, C. F. (2016). Understanding
499 Heterogeneity in Clinical Cohorts Using Normative Models: Beyond Case-Control Studies.
500 *Biological Psychiatry*, 80(7), 552–561. <https://doi.org/10.1016/j.biopsych.2015.12.023>

503 Marquand, A. F., Wolfers, T., Mennes, M., Buitelaar, J., & Beckmann, C. F. (2016). Beyond
504 Lumping and Splitting: A Review of Computational Approaches for Stratifying Psychiatric
505 Disorders. *Biological Psychiatry: Cognitive Neuroscience and Neuroimaging*, 1(5), 433–
506 447. <https://doi.org/10.1016/j.bpsc.2016.04.002>

507 Martinussen, M., Fischl, B., Larsson, H. B., Skranes, J., Kulseng, S., Vangberg, T. R., Vik, T.,
508 Brubakk, A.-M., Haraldseth, O., & Dale, A. M. (2005). Cerebral cortex thickness in 15-year-
509 old adolescents with low birth weight measured by an automated MRI-based method.
510 *Brain*, 128(11), 2588–2596. <https://doi.org/10.1093/brain/awh610>

511 Mills, K. L., Siegmund, K. D., Tamnes, C. K., Ferschmann, L., Wierenga, L. M., Bos, M. G. N.,
512 Luna, B., Li, C., & Herting, M. M. (2021). Inter-individual variability in structural brain
513 development from late childhood to young adulthood. *NeuroImage*, 242(August), 118450.
514 <https://doi.org/10.1016/j.neuroimage.2021.118450>

515 Nagy, Z., Lagercrantz, H., & Hutton, C. (2011). Effects of Preterm Birth on Cortical Thickness
516 Measured in Adolescence. *Cerebral Cortex*, 21(2), 300–306.
517 <https://doi.org/10.1093/cercor/bhq095>

518 Pan, S. J., & Yang, Q. (2010). A Survey on Transfer Learning. *IEEE Transactions on
519 Knowledge and Data Engineering*, 22(10), 1345–1359.
520 <https://doi.org/10.1109/TKDE.2009.191>

521 Pereira, J. B., Ibarretxe-Bilbao, N., Marti, M. J., Compta, Y., Junqué, C., Bargallo, N., & Tolosa,
522 E. (2012). Assessment of cortical degeneration in patients with Parkinson's disease by
523 voxel-based morphometry, cortical folding, and cortical thickness. *Human Brain Mapping*,
524 33(11), 2521–2534. <https://doi.org/10.1002/hbm.21378>

525 Remiszewski, N., Bryant, J. E., Rutherford, S. E., Marquand, A. F., Nelson, E., Askar, I., Lahti,
526 A. C., & Kraguljac, N. V. (2022). Contrasting Case-Control and Normative Reference
527 Approaches to Capture Clinically Relevant Structural Brain Abnormalities in Patients With
528 First-Episode Psychosis Who Are Antipsychotic Naïve. *JAMA Psychiatry*, 79(11), 1133.
529 <https://doi.org/10.1001/jamapsychiatry.2022.3010>

530 Rogers, J. C., & de Brito, S. A. (2016). Cortical and subcortical gray matter volume in youths
531 with conduct problems ameta-Analysis. *JAMA Psychiatry*, 73(1), 64–72.
532 <https://doi.org/10.1001/jamapsychiatry.2015.2423>

533 Rutherford, S., Fraza, C., Dinga, R., Kia, S. M., Wolfers, T., Zabihi, M., Berthet, P., Worker, A.,
534 Verdi, S., Andrews, D., Han, L. K. M., Bayer, J. M. M., Dazzan, P., McGuire, P., Mocking,
535 R. T., Schene, A., Sripada, C., Tso, I. F., Duval, E. R., ... Marquand, A. F. (2022). Charting

536 brain growth and aging at high spatial precision. *ELife*, 11, 1–15.
537 <https://doi.org/10.7554/eLife.72904>

538 Rutherford, S., Kia, S. M., Wolfers, T., Fraza, C., Zabihi, M., Dinga, R., Berthet, P., Worker, A.,
539 Verdi, S., Ruhe, H. G., Beckmann, C. F., & Marquand, A. F. (2022). The normative
540 modeling framework for computational psychiatry. *Nature Protocols*, 17(July).
541 <https://doi.org/10.1038/s41596-022-00696-5>

542 Solmi, M., Radua, J., Olivola, M., Croce, E., Soardo, L., Salazar de Pablo, G., il Shin, J.,
543 Kirkbride, J. B., Jones, P., Kim, J. H., Kim, J. Y., Carvalho, A. F., Seeman, M. v., Correll, C.
544 U., & Fusar-Poli, P. (2022). Age at onset of mental disorders worldwide: large-scale meta-
545 analysis of 192 epidemiological studies. *Molecular Psychiatry*, 27(1), 281–295.
546 <https://doi.org/10.1038/s41380-021-01161-7>

547 Tamnes, C. K., Herting, M. M., Goddings, A. L., Meuwese, R., Blakemore, S. J., Dahl, R. E.,
548 Güroğlu, B., Raznahan, A., Sowell, E. R., Crone, E. A., & Mills, K. L. (2017). Development
549 of the cerebral cortex across adolescence: A multisample study of inter-related longitudinal
550 changes in cortical volume, surface area, and thickness. *Journal of Neuroscience*, 37(12),
551 3402–3412. <https://doi.org/10.1523/JNEUROSCI.3302-16.2017>

552 Thambisetty, M., Wan, J., Carass, A., An, Y., Prince, J. L., & Resnick, S. M. (2010). Longitudinal
553 changes in cortical thickness associated with normal aging. *NeuroImage*, 52(4), 1215–
554 1223. <https://doi.org/10.1016/j.neuroimage.2010.04.258>

555 Volpe, J. J. (2009). Brain injury in premature infants: a complex amalgam of destructive and
556 developmental disturbances. In *The Lancet Neurology* (Vol. 8, Issue 1, pp. 110–124).
557 [https://doi.org/10.1016/S1474-4422\(08\)70294-1](https://doi.org/10.1016/S1474-4422(08)70294-1)

558 White, T., Muetzel, R. L., el Marroun, H., Blanken, L. M. E., Jansen, P., Bolhuis, K., Kocevska,
559 D., Mous, S. E., Mulder, R., Jaddoe, V. W. V., van der Lugt, A., Verhulst, F. C., & Tiemeier,
560 H. (2018). Paediatric population neuroimaging and the Generation R Study: the second
561 wave. *European Journal of Epidemiology*, 33(1), 99–125. <https://doi.org/10.1007/s10654-017-0319-y>

562 Whittle, S., Vijayakumar, N., Simmons, J. G., & Allen, N. B. (2020). Internalizing and
563 Externalizing Symptoms Are Associated With Different Trajectories of Cortical
564 Development During Late Childhood. *Journal of the American Academy of Child and
565 Adolescent Psychiatry*, 59(1), 177–185. <https://doi.org/10.1016/j.jaac.2019.04.006>

566 Zabihi, M., Oldehinkel, M., Wolfers, T., Frouin, V., Goyard, D., Loth, E., Charman, T., Tillmann,
567 J., Banaschewski, T., Dumas, G., Holt, R., Baron-Cohen, S., Durston, S., Bölte, S.,
568 Murphy, D., Ecker, C., Buitelaar, J. K., Beckmann, C. F., & Marquand, A. F. (2019).
569

570 Dissecting the Heterogeneous Cortical Anatomy of Autism Spectrum Disorder Using
571 Normative Models. *Biological Psychiatry: Cognitive Neuroscience and Neuroimaging*, 4(6),
572 567–578. <https://doi.org/10.1016/j.bpsc.2018.11.013>

573 Zhao, Y., Zhang, Q., Shah, C., Li, Q., Sweeney, J. A., Li, F., & Gong, Q. (2022). Cortical
574 Thickness Abnormalities at Different Stages of the Illness Course in Schizophrenia. *JAMA
575 Psychiatry*, 79(6), 560. <https://doi.org/10.1001/jamapsychiatry.2022.0799>

576 Zubiaurre-Elorza, L., Soria-Pastor, S., Junque, C., Sala-Llonch, R., Segarra, D., Bargallo, N., &
577 Macaya, A. (2012). Cortical Thickness and Behavior Abnormalities in Children Born
578 Preterm. *PLoS ONE*, 7(7), e42148. <https://doi.org/10.1371/journal.pone.0042148>

579

580

581

582

583

584

585

586

587

588

589

590

591

592

593

594

595

596

597

598

599

600

601

602

603